EVOLUTION OF DIRECTIONAL WAVE SPECTRA THROUGH FINITE REGULAR AND RANDOMLY-PERTURBED ARRAYS OF SCATTERERS

FABIEN MONTIEL[†*], VERNON A. SQUIRE[‡*], AND LUKE G. BENNETTS[§]

Abstract. A method is proposed to solve the full linear problem of wave scattering by a large finite array of circular inclusions in two spatial dimensions and compute the concomitant evolution of directional wave properties through the array. The method decomposes the array into slabs. Interactions between adjacent slabs are calculated using a representation of the wave fields scattered by each slab as integrals of plane waves over the directional spectrum plus exponentially decaying branches. The method is applied to the canonical problem of acoustic sound-hard scatterers. Validation is sought for: (i) regular arrays via comparison with solutions of corresponding infinite, periodic single- and multiple-row arrays; and (ii) random arrays via comparison with Foldy's approximation for the effective field. A numerical investigation is conducted to determine the effect of introducing random perturbations into regular arrays on the directional properties of the reflected and transmitted fields.

Key words. multiple scattering, directional spectrum, random array

AMS subject classifications. 31A05, 31A10, 31A25, 35J05, 35J25, 35Q35, 42A10, 74J20

1. Introduction. Two-dimensional scattering of linear time-harmonic waves by large arrays of inclusions forms the basis of many idealized multiple scattering problems in areas as varied as optics, acoustics, elasticity and hydrodynamics. Examples include the study of electromagnetic (EM) waves in photonic crystals (McPhedran et al. [19]), acoustic waves in phononic crystals (Vasseur et al. [30]), flexural waves in a plate with circular cavities (Parnell and Martin [22]) and water wave interactions with offshore structures (Kagemoto and Yue [13]). Martin [18] provides an extensive review of mathematical methods developed to solve such multiple scattering problems.

Our investigation is motivated by the study of ocean wave propagation through large arrays of floating ice floes, in the marginal ice zones (MIZs) that form at the outer edges of the sea-ice-covered oceans. Attenuation of wave energy with distance traveled into the MIZ, and the concomitant broadening of the directional spectrum have been observed, and attributed to scattering (Wadhams et al. [31]).

Modeling the evolution of the directional and energetic wave properties through large arrays of ice floes has proved challenging, and even the few most recent attempts to do so are based on significant simplifications of multiple scattering effects. A popular approach consists of modelling the ice cover by an infinite array of scatterers, with some artificial regular spacing/periodicity assumption applied (Bennetts and Squire [4], Peter and Meylan [23], Bennetts et al. [3]). Specifically, the scatterers are arranged into periodic rows (referred to as a multiple-row array), so the wave directional properties are known between rows throughout the array.

[†]Corresponding author. Department of Mathematics and Statistics, University of Otago, P.O. Box 56, Dunedin, 9054, New Zealand (fmontiel@maths.otago.ac.nz).

[‡]Department of Mathematics and Statistics, University of Otago, P.O. Box 56, Dunedin, 9054, New Zealand (vernon.squire@otago.ac.nz).

[*]FM and VS are supported by the Office of Naval Research Departmental Research Initiative 'Sea State and Boundary Layer Physics of the Emerging Arctic Ocean' (award number N00014-131-0279) and the University of Otago.

[§]School of Mathematical Sciences, University of Adelaide, Adelaide, South Australia 5005, Australia (luke.bennetts@adelaide.edu.au). LB acknowledges funding support from the Australian Research Council (DE130101571) and the Australian Antarctic Science Grant Program (Project 4123).

In a regular lattice, where all rows are identical, interference mechanisms lead to stopband/passband structures (Brillouin [6]). Disorder can be included in different ways, e.g. varying the spacing between rows randomly (Bennetts and Squire [4]) or taking a random periodic pattern for each row, given a common spatial period (Peter and Meylan [23]; a method originally used to model photonic crystals by McPhedran et al. [19]). The rate of wave energy attenuation is calculated from an ensemble average of random realisations of the array. However, the periodicity in each row introduces limitations because waves can only travel in certain directions, the so-called scattering angles, so these approaches cannot be used to estimate the evolution of the directional wave properties. Bennetts [2] partially relaxed this restriction allowing for different periodicities in the rows, so that multiple scattering effects between rows lead to a continuous spectrum of directions in which waves can travel.

We propose a novel method to compute the evolution of directional wave properties through a large finite array of scatterers in two dimensions. The method is presented for circular acoustic sound-hard scatterers. It uses a clustering of the array into parallel slabs, and therefore takes advantage of the multiple-row array approach used for infinite rows, whilst alleviating the constraints of regularity within the rows.

Our method provides a numerical solution to multiple scattering by large finite arrays, e.g. O $\left(10^3\text{–}10^4\right)$ scatterers, but differs significantly from existing approaches, e.g. the order-of-scattering method (Twersky [27]), the scatterer polymerization technique (Cai and Williams [7]) and the fast multipole method (FMM; Cheng et al. [8]; Lai et al. [15]). The two former existing methods provide improvements but have convergence issues as discussed by Martin [18]. The FMM has offered the most significant improvements in terms of efficiency, accuracy and its ability to consider large arrays, but does not provide a natural framework to analyze directional properties of the wave field through the array. Although our clustering technique cannot claim to match the efficiency of the FMM, the two methods can be combined to improve the efficiency of our technique. This idea will not be explored here, however, as the focus of the current paper is different.

We adopt the directional spectrum approach of Bennetts [2], which defines the wave field as a superposition of plane waves with amplitudes that depend continuously on the direction. This allows us to describe the wave field on either side of a row of scatterers as an amplitude function of the angular parameter; the so-called directional spectrum. The method used to calculate the directional spectra differs significantly from that of Bennetts [2], however. First, the solution is found in the form of expansions of cylindrical harmonics using separation of variables in polar coordinates. The second step consists of transforming each circular wave form (cylindrical harmonics) into a continuous superposition of plane waves. This polar-to-Cartesian mapping is provided by Sommerfeld's integral representation of the Hankel function (Sommerfeld [26], §19), in which the integration over the angular parameter extends into the complex plane.

The plane wave integral representation of the cylindrical harmonics forms the basis of different methods to solve various two-dimensional multiple scattering problems. The so-called Twersky's method (see Twersky [29]) makes use of this integral representation to express the scattered far-field due to arbitrarily many cylinders as a directional spectrum of plane waves. The directional spectra due to all the scatterers are the solutions of a self-consistent system of integral equations that involve the scattering function of each scatterer in isolation. The method was extended by Millar in a series of papers to solve a number of scattering problems involving identical

obstructions (see, e.g., Millar [20] for the finite array problem).

Multiple-row array methods are efficient and stable as the number of rows increases. They are based on the recursive scattering matrix (S-matrix) method, which was developed by Ko and Sambles [14] in the context of wave propagation in layered media to overcome the stability issues of the transfer matrix (T-matrix) method (see, e.g., Yeh [33]). We note that other stable schemes were devised to remedy numerical issues of the naive application the T-matrix method (see, e.g., Schwartz and DeSandre [24]; Moharam et al. [21]). The S-matrix method has been broadly used to model, for example, EM wave propagation in multilayer periodic gratings (see Cotter et al. [10]; Li [16]) and photonic crystals (see McPhedran et al. [19]).

In our context, we then seek a solution to the reflection/transmission problem for each slab in the form of a S-matrix which maps incident wave amplitudes to the corresponding reflected/transmitted wave amplitudes. We use the plane wave representation of the cylindrical harmonics to derive the reflected and transmitted (plane wave) directional spectra by a slab of arbitrary scatterers due to an arbitrary incident spectrum. Our method resembles that proposed by Frezza et al. [12] and Lai et al. [15] in the context of EM wave scattering by dielectric inclusions embedded in a dielectric slab, although we extend these investigations by considering multiple slabs. This allows us to track the evolution of the directional properties of the wave field through the array.

We refer to the method described in this paper as the slab-clustering technique. Considering a large finite array of scatterers, (i) we divide the domain into slab clusters, each containing a smaller number of scatterers; (ii) we solve the multiple scattering problem within each slab using a self-consistent approach; (iii) we transform the scattered field into reflected and transmitted spectra of plane waves; and (iv) we combine all the slabs using multiple-row array techniques. A discretization of the angular domain, similar to that performed by Bennetts [2], yields a numerical solution for the directional spectra of plane waves at each slab boundary.

We use the method to show the extent to which the solution to the finite array problem approximates the response due to infinite regular and random arrays. Further, we investigate the effect of introducing random perturbation in a regular arrangement of scatterers on the directional properties of the scattered field using Monte-Carlo simulations.

2. Preliminaries. We consider a simple setting for wave scattering in an infinite plane described by the Cartesian coordinates $\mathbf{x} = (x, y)$. The plane includes an arbitrary arrangement of J non-overlapping sound-hard obstructions, with circular boundaries. Each obstruction j (for $1 \leq j \leq J$) is defined by its radius a_j and the location of its centre (x_j, y_j) in the Cartesian reference frame. We assume that $(x_1, y_1) = (0, 0)$ and $x_j > 0$ for all $j \geq 2$, without loss of generality. Figure 1a shows an example array.

A time-harmonic potential field $\mathrm{Re}\{\phi(\mathbf{x})\,\mathrm{e}^{-\,\mathrm{i}\omega t}\}$ with angular frequency ω is defined everywhere in the domain exterior to the obstructions, denoted by Ω. The complex (reduced) potential $\phi(\mathbf{x})$ is governed by Helmholtz equation

$$\nabla^2\phi + k^2\phi = 0 \quad (\mathbf{x} \in \Omega), \tag{2.1}$$

where the wavenumber k is a real positive constant that depends on frequency. Letting Γ_j denote the boundary of each obstruction j, we prescribe a Neumann boundary condition

$$\partial_n\phi = 0 \quad (\mathbf{x} \in \Gamma_j), \tag{2.2}$$

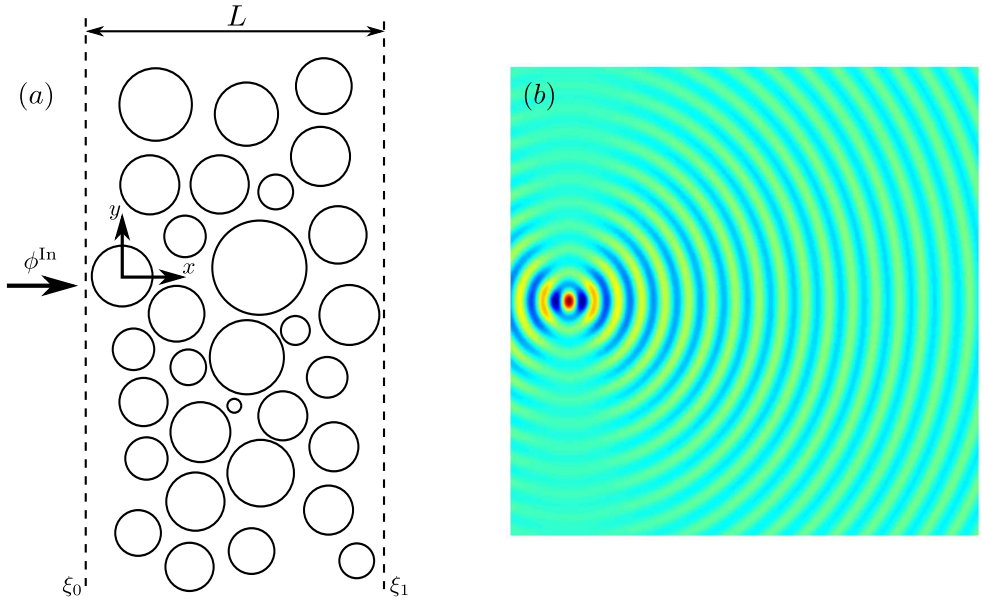

FIG. 1. *(a) Schematic diagram of the finite arbitrary array contained in a slab of width L. (b) Real part of the incident field* ϕ^{In} *for an incident angular spectrum* $A^{\mathrm{In}}(\tau) = \cos\tau$ *in the region* $(x, y) \in [-5, 35] \times [-20, 20]$.

on all circular contours ($1 \leq j \leq J$).

We define the wave forcing as a continuous directional spectrum of plane waves traveling towards $x \to \infty$. This may be expressed as an integral of plane waves with amplitudes that depend continuously on the angle τ (with respect to the x-axis) in which the waves travel, i.e.

$$\phi^{\mathrm{In}}(\mathbf{x}) = \int_{-\pi/2}^{\pi/2} A^{\mathrm{In}}(\tau)\, \mathrm{e}^{\,\mathrm{i}k(x\cos\tau + y\sin\tau)}\, \mathrm{d}\tau. \tag{2.3}$$

The incident wave directional spectrum $A^{\mathrm{In}}(\tau)$ characterizes the angular distribution of incoming energy at the origin. It is an arbitrary function of the angular parameter $\tau \in [-\pi/2, \pi/2]$. In particular, we can simulate a unidirectional incident wave traveling at angle τ_0 with respect to the x-axis and with unit amplitude by setting $A^{\mathrm{In}}(\tau) = \delta(\tau - \tau_0)$, where δ is the Dirac delta function.

It is helpful to visualize the incident field with spectrum $A^{\mathrm{In}}(\tau) = \cos\tau$, which will be the default forcing for the results presented in §7. Figure 1b shows the real part of ϕ^{In} for $k = \pi$ and $(x, y) \in [-5, 35] \times [-20, 20]$. Plane waves traveling from left to right at angle τ with amplitude $\cos\tau$ coherently superpose and peak at the origin. Note the rapid decay of wave amplitude for increasing $|y|$ at $x = 0$.

Our goal is to characterize the reflected and transmitted components of the wave field as directional spectra analogous to the incident field in (2.3). The method, which will be described in §4, requires the solution of the multiple scattering problem. The multipole method, based on separation of variables in polar coordinates (Martin [18]), is used for this purpose, so a polar-to-Cartesian mapping will be needed to define the reflection and transmission properties of the wave field.

We introduce the local polar coordinates (r_j, θ_j) associated with each circular obstruction j and define $(r, \theta) = (r_1, \theta_1)$ as the global polar coordinates. These are

related to the Cartesian coordinates through the relationships $x = x_j + r_j \cos\theta_j$ and $y = y_j + r_j \sin\theta_j$. We express the radiation condition for the finite array of scatterers in the global polar coordinate system, as

$$r^{1/2}\,(\partial/\partial_r - \mathrm{i}k)\,\phi^{\mathrm{S}} \to 0 \quad (r \to \infty), \tag{2.4}$$

where $\phi^{\mathrm{S}} = \phi - \phi^{\mathrm{In}}$ is the scattered wave potential.

To solve the multiple scattering problem, we express the incident wave potential in the local polar coordinates associated with an arbitrary obstruction j. We obtain the following truncated Fourier-type expansion

$$\phi^{\mathrm{In}}(r_j, \theta_j) \approx \sum_{n=-N}^{N} f_n^{(j)} \mathrm{J}_n(kr_j)\,\mathrm{e}^{\,\mathrm{i}n\theta_j}, \tag{2.5}$$

where J_n denotes the Bessel function of the first kind of order n, and

$$f_n^{(j)} = \mathrm{i}^n \int_{-\pi/2}^{\pi/2} A^{\mathrm{In}}(\tau)\,\mathrm{e}^{-\,\mathrm{i}n\tau}\,\mathrm{e}^{\,\mathrm{i}k(x_j\cos\tau + y_j \sin\tau)}\,\mathrm{d}\tau. \tag{2.6}$$

Under a given wave forcing, each obstruction j produces a scattered wave field, expressed as a partial sum of polar harmonics

$$\phi_j^{\mathrm{S}}(r_j, \theta_j) \approx \sum_{n=-N}^{N} c_n^{(j)} \mathrm{H}_n(kr_j)\,\mathrm{e}^{\,\mathrm{i}n\theta_j}, \tag{2.7}$$

where H_n denotes the Hankel function of the first kind of order n. A numerical solution for $c_n^{(j)}$ is found using the multipole method for finite arrays (see, e.g., Martin [18], §4.5). A summary of the method is given in Appendix A.

We obtain a diffraction transfer operator $\mathfrak{D}$ of order $J(2N+1)$ mapping incident to scattered field amplitudes, i.e.

$$\mathbf{c} = \mathfrak{D}\mathbf{f}, \tag{2.8}$$

where $\mathbf{c}$ and $\mathbf{f}$ are column vectors of length $J(2N+1)$ with entries $c_n^{(j)}$ and $f_n^{(j)}$. The matrix $\mathfrak{D}$ is found by inversion of the system derived in Appendix A. Alternatively, the FMM could be used to obtain $\mathfrak{D}$ at a lower computational cost (see, e.g., Lai et al. [15]). The diffraction transfer operator characterizes the system fully in terms of local polar wave expansions.

3. Plane wave expansion of cylindrical harmonics. We seek to transform the cylindrical harmonics $\mathrm{H}_n(kr)\,\mathrm{e}^{\,\mathrm{i}n\theta}$ for $n \in \mathbb{Z}$ into directional spectra composed of plane waves. Such a plane wave representation is given by Cincotti et al. [9] in the context of electromagnetic wave scattering. It is based on Sommerfeld's integral representation of the Hankel function of the first kind (Sommerfeld [26])

$$\mathrm{H}_n(kr) = \frac{(-\mathrm{i})^n}{\pi} \int_C \exp(\,\mathrm{i}kr\cos w + \,\mathrm{i}nw)\,\mathrm{d}w,$$

where C is the integration path, which must be chosen in the complex plane such that (i) it passes through the origin, (ii) its lower limit is $\gamma_l + \mathrm{i}\infty$, with $-\pi < \gamma_l < 0$, and (iii) its upper limit is $\gamma_u - \mathrm{i}\infty$, with $0 < \gamma_u < \pi$. Choosing $\gamma_l = -\pi/2 - \theta$

and $\gamma_u = \pi/2 - \theta$ if $x \geq 0$, and $\gamma_l = \pi/2 - \theta$ and $\gamma_u = 3\pi/2 - \theta$ if $x \leq 0$, with an appropriate substitution, we obtain

$$\mathrm{H}_n(kr)\,\mathrm{e}^{\,\mathrm{i}n\theta} = \begin{cases} \dfrac{(-\mathrm{i})^n}{\pi} \displaystyle\int_{-\pi/2+\,\mathrm{i}\infty}^{\pi/2-\,\mathrm{i}\infty} \mathrm{e}^{\,\mathrm{i}n\chi}\,\mathrm{e}^{\,\mathrm{i}k(x\cos\chi + y\sin\chi)}\,\mathrm{d}\chi, & (x \geq 0) \\ \dfrac{\mathrm{i}^n}{\pi} \displaystyle\int_{-\pi/2+\,\mathrm{i}\infty}^{\pi/2-\,\mathrm{i}\infty} \mathrm{e}^{-\,\mathrm{i}n\chi}\,\mathrm{e}^{\,\mathrm{i}k(-x\cos\chi + y\sin\chi)}\,\mathrm{d}\chi, & (x \leq 0). \end{cases} \tag{3.1}$$

Equation (3.1) expresses the cylindrical harmonic as a continuous angular spectrum of plane waves. The first and second expressions characterize wave fields traveling in the positive and negative x directions, respectively. In response to an incident field traveling in the positive x direction, these would correspond to the transmitted and reflected fields, respectively.

Inspection of the integrands in (3.1) for complex values of χ shows that the plane wave term decays exponentially with x, and the larger the imaginary part of χ the faster the decay. These components correspond to evanescent waves, which may be neglected in the far field, i.e. when $|x| \to \infty$. The approximation consisting of neglecting the evanescent waves in the near field is often called the wide-spacing approximation (WSA). It can easily be implemented by reducing the domain of integration to $(-\pi/2, \pi/2)$. We will demonstrate in §7, however, that the complex branches of the integration domain in (3.1) may have a significant influence, so that the WSA is not always suitable for this problem.

4. Reflection and transmission by a slab. The analysis conducted in §3 suggests that we express the reflected and transmitted fields due to each obstruction at fixed values of x. Let Ω_s define an infinite vertical region of finite width, parallel to the y-axis and containing the centre of all the scatterers, i.e. $\Omega_s = \{\mathbf{x} \in \Omega : \xi_0 \leq x \leq \xi_1\}$, where $\xi_0 \leq 0$ and $\xi_1 \geq \max(x_j : 1 \leq j \leq J)$ can be chosen arbitrarily (see figure 1a). The region Ω_s will be referred to as a slab and $L = \xi_1 - \xi_0$ defines its width. We now seek the scattered wave field in the form of a field reflected and transmitted by the slab, i.e.

$$\phi^{\mathrm{R}}(\mathbf{x}) = \int_{-\pi/2+\,\mathrm{i}\infty}^{\pi/2-\,\mathrm{i}\infty} A^{\mathrm{R}}(\chi)\,\mathrm{e}^{\,\mathrm{i}k(-(x-\xi_0)\cos\chi + y\sin\chi)}\,\mathrm{d}\chi \quad (x \leq \xi_0), \quad \text{and} \tag{4.1a}$$

$$\phi^{\mathrm{T}}(\mathbf{x}) = \int_{-\pi/2+\,\mathrm{i}\infty}^{\pi/2-\,\mathrm{i}\infty} A^{\mathrm{T}}(\chi)\,\mathrm{e}^{\,\mathrm{i}k((x-\xi_1)\cos\chi + y\sin\chi)}\,\mathrm{d}\chi \quad (x \geq \xi_1), \tag{4.1b}$$

where the reflected and transmitted spectra $A^{\mathrm{R}}(\chi)$ and $A^{\mathrm{T}}(\chi)$ are unknown. For $|x|$ sufficiently large, the WSA holds and the integration domain may be reduced to $(-\pi/2, \pi/2)$, as explained in §3.

The reflected spectrum $A^{\mathrm{R}}(\chi)$ describes the angular distribution of the traveling wave field at $\mathbf{x} = (\xi_0, 0)$ propagating in the negative x direction. Likewise, the transmitted spectrum $A^{\mathrm{T}}(\chi)$ represents the angular distribution at $\mathbf{x} = (\xi_1, 0)$ of the wave field traveling in the positive x direction. It is composed of the transmitted component of the scattered field and the incident field, so can be written as $A^{\mathrm{T}}(\chi) = \widetilde{A}^{\mathrm{T}}(\chi) + \mathrm{e}^{\,\mathrm{i}k\xi_1\cos\chi} A^{\mathrm{In}}(\chi)$, accounting for the appropriate phase change.

The spectra $A^{\mathrm{R}}(\chi)$ and $A^{\mathrm{T}}(\chi)$ can be expressed via integral mappings of the incident spectrum as

$$A^{\mathrm{R}}(\chi) = \int_{-\pi/2}^{\pi/2} \mathcal{R}(\chi : \tau) A^{\mathrm{In}}(\tau)\,\mathrm{d}\tau \quad \text{and} \quad A^{\mathrm{T}}(\chi) = \int_{-\pi/2}^{\pi/2} \mathcal{T}(\chi : \tau) A^{\mathrm{In}}(\tau)\,\mathrm{d}\tau, \tag{4.2}$$

where $\mathcal{R}(\chi:\tau)$ and $\mathcal{T}(\chi:\tau)$ are the reflection and transmission kernels, respectively. Note that the integration domain need not include the imaginary branches here, as the incident field is purely traveling. The kernel functions fully characterize the system as they map an arbitrary incident spectrum to the corresponding reflected and transmitted spectra. In particular, $\mathcal{R}(\chi:\tau_0)$ and $\mathcal{T}(\chi:\tau_0)$ represent the reflected and transmitted spectra due to a unidirectional incident plane wave traveling at an angle τ_0 with respect to the x-axis, i.e. for $A^{\mathrm{In}}(\tau)=\delta(\tau-\tau_0)$.

Using the solution of the multiple scattering problem described in the previous section, we can find semi-analytical expressions for the kernel functions. The procedure is described here for the transmitted field. For each obstruction j, we express the scattered field (2.7) using the plane wave decomposition of the cylindrical wave form for $x\geq 0$ given in (3.1). We obtain

$$\phi_j^{\mathrm{S}}(x,y)\approx\int_{-\pi/2+\mathrm{i}\infty}^{\pi/2-\mathrm{i}\infty}\left(\sum_n\frac{(-\mathrm{i})^n}{\pi}c_n^{(j)}\,\mathrm{e}^{\,\mathrm{i}n\chi}\right)\mathrm{e}^{\,\mathrm{i}k((x-x_j)\cos\chi+(y-y_j)\sin\chi)}\,\mathrm{d}\chi,$$

valid for $x\geq x_j$. We then use (2.8) and (2.6) in turn, to write the amplitudes $c_n^{(j)}$ in terms of the incident spectrum $A^{\mathrm{In}}(\tau)$. The transmission kernel is finally obtained by superposing the contribution of all obstructions (i.e. summing over j) and accounting for the phase change required to align the phase reference for all obstructions at $\mathbf{x}=(\xi_1,0)$. Using vector and matrix notations, we obtain after some algebra

$$\mathcal{T}(\chi:\tau)=\left(\mathbf{V}^{\mathrm{T}}(\chi)\right)^{\mathrm{tr}}\mathfrak{D}\mathbf{V}^{\mathrm{In}}(\tau)+\,\mathrm{e}^{\,\mathrm{i}k\xi_1\cos\chi}\delta(\chi-\tau),\tag{4.3}$$

where $\mathbf{V}^{\mathrm{T}}(\chi)$ and $\mathbf{V}^{\mathrm{In}}(\tau)$ are column vectors of length $J(2N+1)$ with entries

$$\left[\mathbf{V}^{\mathrm{T}}(\chi)\right]_{(j-1)(2N+1)+N+n+1}=\frac{(-\mathrm{i})^n}{\pi}\,\mathrm{e}^{-\,\mathrm{i}k((x_j-\xi_1)\cos\chi+y_j\sin\chi)}\,\mathrm{e}^{\,\mathrm{i}n\chi},$$

$1\leq j\leq J$, $-N\leq n\leq N$, and

$$\left[\mathbf{V}^{\mathrm{In}}(\tau)\right]_{(p-1)(2N+1)+N+s+1}=\mathrm{i}^s\,\mathrm{e}^{\,\mathrm{i}k(x_p\cos\tau+y_p\sin\tau)}\,\mathrm{e}^{-\,\mathrm{i}s\tau},$$

$1\leq p\leq J$, $-N\leq s\leq N$, and the superscript tr indicates matrix transpose. The second term in (4.3) represents the contribution from the incident field.

In a similar fashion, we derive an expression for the reflection kernel

$$\mathcal{R}(\chi:\tau)=\left(\mathbf{V}^{\mathrm{R}}(\chi)\right)^{\mathrm{tr}}\mathfrak{D}\mathbf{V}^{\mathrm{In}}(\tau),\tag{4.4}$$

where the column vector $\mathbf{V}^{\mathrm{R}}(\chi)$ of length $J(2N+1)$ has entries

$$\left[\mathbf{V}^{\mathrm{R}}(\chi)\right]_{(j-1)(2N+1)+N+n+1}=\frac{\mathrm{i}^n}{\pi}\,\mathrm{e}^{\,\mathrm{i}k((x_j-\xi_0)\cos\chi-y_j\sin\chi)}\,\mathrm{e}^{-\,\mathrm{i}n\chi}.$$

We note that these formulas are valid for $\xi_0\leq x_j\leq\xi_1$, $1\leq j\leq J$, so the centre of each scatterer only is required to be contained in the slab. In particular, the method is still valid if the boundary of a scatterer intersects with the boundary of a slab.

5. Numerical method. We now approximate the transmission and reflection kernels given by (4.3) and (4.4) numerically. We seek discrete forms of $\mathcal{T}(\chi:\tau)$ and $\mathcal{R}(\chi:\tau)$ using uniform sampling of the angular domain. This produces a matrix mapping that fully describes the system.

The uniform sampling method consists of discretizing the variables χ and τ to perform numerical integration of (4.1) and (4.2). We sample the complex angular domain along the contour parametrized by $\chi(t) = -\pi/2 - \mathrm{i}(1+t)$, for $t < -1$, $\chi(t) = \pi/2t$, for $-1 \leq t \leq 1$, and $\chi(t) = \pi/2 + \mathrm{i}(1-t)$, for $t > 1$. Numerical integration requires that we truncate the limits to $-\pi/2 + \gamma\,\mathrm{i}$ and $\pi/2 - \gamma\,\mathrm{i}$, where $\gamma \geq 0$, which is appropriate considering that the integrands decay exponentially faster as γ increases. The parameter γ is then chosen to ensure convergence of the improper integrals. We select $2N_s + 1$ samples χ_i ,$-N_s \leq i \leq N_s$, from the truncated contour and define the column vectors $\mathbf{A}^{\mathrm{In}}$, $\mathbf{A}^{\mathrm{R}}$ and $\mathbf{A}^{\mathrm{T}}$ of length $2N_s + 1$, containing the values of the incident, reflected and transmitted spectra, respectively, at these angular samples. We seek to compute square matrices $\mathfrak{R}$ and $\mathfrak{T}$ of size $2N_s + 1$, such that

$$\mathbf{A}^{\mathrm{R}} = \mathfrak{R}\mathbf{A}^{\mathrm{In}} \quad \text{and} \quad \mathbf{A}^{\mathrm{T}} = \mathfrak{T}\mathbf{A}^{\mathrm{In}}. \tag{5.1}$$

Therefore, we discretize the integral mappings given in (4.2), using the trapezoidal rule with a non-uniform grid, due to the mix of real and complex samples, to approximate the integrals. Sampling the kernel functions at the angles selected above, we then obtain the discrete maps of (5.1) in a straightforward manner.

The numerical scheme described here was found to converge as $\mathrm{O}\left(N_s^{-4}\right)$. We note that the trapezoidal rule is particularly robust for integrating noisy directional spectra. Higher order schemes, e.g. a Gaussian quadrature with special sampling (see Borghi *et al.* [5]), were found to perform poorly compared to the trapezoidal rule for strongly scattering arrays. Higher efficiency may be obtained by using more advanced numerical schemes, such as the non-uniform fast Fourier transform (see Lai *et al.* [15] for an application to a similar problem with EM waves), but the simplicity and robustness of our scheme was preferred in this case.

6. Multiple slabs. We now seek to determine the evolution of the directional spectrum through very large arrays. The method is based on clustering the full array into slabs, so we can apply a multiple row interaction technique. We note that the multipole method described in §2 was found to be impractical for more than $\mathrm{O}\,(100)$ scatterers, due to the numerical cost of computing the diffraction transfer matrix $\mathfrak{D}$ by inversion of the large system (A.3). Consequently, the slab-clustering method provides an effective means of increasing the number of scatterers, with no restrictions on the spacing or size of scatterers.

Consider M adjacent slabs $\Omega_s^{(q)} = \{\mathbf{x} \in \Omega : \xi_{q-1} \leq x \leq \xi_q\}$, $1 \leq q \leq M$, with width $L_q = \xi_q - \xi_{q-1}$. Each slab contains the centres of arbitrarily many circular obstructions, J_q say. The system is forced to respond under an incident field of the form given by (2.3) and we consider multiple scattering effects between the slabs. As a consequence, we describe the potential field between two adjacent slabs as the coherent superposition of left-traveling and right-traveling directional spectra. The field at $x = \xi_q$ can be expressed as

$$\phi_q(\mathbf{x}) = \int_{-\pi/2+\mathrm{i}\infty}^{\pi/2-\mathrm{i}\infty} \Big(A_q^+(\chi)\,\mathrm{e}^{\,\mathrm{i}k((x-\xi_q)\cos\chi + y\sin\chi)} + A_q^-(\chi)\,\mathrm{e}^{\,\mathrm{i}k(-(x-\xi_q)\cos\chi + y\sin\chi)} \Big)\,\mathrm{d}\chi, \tag{6.1}$$

$0 \leq q \leq M$, where $A_q^+(\chi)$ and $A_q^-(\chi)$ represent the right- and left-traveling directional spectra, respectively. The forcing terms are given by $A_0^+(\chi) = A^{\mathrm{In}}(\chi)\,\mathrm{e}^{\,\mathrm{i}k\xi_0\cos\chi}$ and $A_M^-(\chi) = 0$, and all the other spectra $A_q^{\pm}(\chi)$ are unknowns of the problem.

The method used to couple the wave interaction effects of all slabs is essentially the same as that used by Bennetts [2] for multiple rows of infinite regular arrays. Each wave spectrum is emitted from a slab by the superposition of a reflection process due to a spectrum incident on the slab and traveling in the opposite direction, and a transmission process, due to an incident spectrum traveling in the same direction. Using similar notations as in §4, the wave spectra at the boundary $x = \xi_q$ are then coupled as follows

$$A_q^+(\chi) = \int_{-\pi/2+\mathrm{i}\infty}^{\pi/2-\mathrm{i}\infty} \left(\mathcal{T}_q^+(\chi:\tau)A_{q-1}^+(\tau) + \mathcal{R}_q^-(\chi:\tau)A_q^-(\tau)\right)\,\mathrm{d}\tau, \tag{6.2a}$$

$$A_q^-(\chi) = \int_{-\pi/2+\mathrm{i}\infty}^{\pi/2-\mathrm{i}\infty} \left(\mathcal{R}_{q+1}^+(\chi:\tau)A_q^+(\tau) + \mathcal{T}_{q+1}^-(\chi:\tau)A_{q+1}^-(\tau)\right)\,\mathrm{d}\tau. \tag{6.2b}$$

The superposition of these reflection and transmission processes requires that we define two reflection kernels and two transmission kernels for each slab, i.e. $\mathcal{R}_q^{\pm}(\chi:\tau)$ and $\mathcal{T}_q^{\pm}(\chi:\tau)$. The $+$ and $-$ superscripts correspond to a wave forcing traveling in the positive and negative x directions, respectively.

The kernel functions $\mathcal{R}_q^+$ and $\mathcal{T}_q^+$, $q = 1,\ldots,M$ are obtained using the method described in §4, being careful to apply the proper phase changes. Calculation of the reflection and transmission kernels due to a wave forcing traveling in the negative x direction needs only very little modification, as they only differ in the phase terms and their expressions follow straightforwardly from the method of §4.

Discretizing (6.2) as in §5 we obtain the following matrix equations

$$\mathbf{A}_q^+ = \mathfrak{T}_q^+\mathbf{A}_{q-1}^+ + \mathfrak{R}_q^-\mathbf{A}_q^- \quad \text{and} \quad \mathbf{A}_q^- = \mathfrak{R}_{q+1}^+\mathbf{A}_q^+ + \mathfrak{T}_{q+1}^-\mathbf{A}_{q+1}^-. \tag{6.3}$$

Column vectors $\mathbf{A}_q^{\pm}$, and square matrices $\mathfrak{R}_q^{\pm}$ and $\mathfrak{T}_q^{\pm}$ are discretized versions of the corresponding spectra, and reflection and transmission kernels, as defined in (5.1).

The solution method for the multiple slab interaction problem is then obtained by combining reflection and transmission matrices of all slabs, using a recursive S-matrix technique. We introduce the reflection and transmission matrices $\mathfrak{R}_{p,q}^{\pm}$ and $\mathfrak{T}_{p,q}^{\pm}$ for the slabs p to q with $p \le q$. They satisfy the relations

$$\mathbf{A}_{p-1}^- = \mathfrak{R}_{p,q}^+\mathbf{A}_{p-1}^+ + \mathfrak{T}_{p,q}^-\mathbf{A}_q^- \quad \text{and} \quad \mathbf{A}_q^+ = \mathfrak{T}_{p,q}^+\mathbf{A}_{p-1}^+ + \mathfrak{R}_{p,q}^-\mathbf{A}_q^-, \tag{6.4}$$

and can be calculated using the following identities

$$\mathfrak{R}_{p,q}^+ = \mathfrak{R}_{p,q-1}^+ + \mathfrak{T}_{p,q-1}^-\left(\mathfrak{I} - \mathfrak{R}_q^+\mathfrak{R}_{p,q-1}^-\right)^{-1}\mathfrak{R}_q^+\mathfrak{T}_{p,q-1}^+,$$

$$\mathfrak{T}_{p,q}^- = \mathfrak{T}_{p,q-1}^-\left(\mathfrak{I} - \mathfrak{R}_q^+\mathfrak{R}_{p,q-1}^-\right)^{-1}\mathfrak{T}_q^-, \quad \mathfrak{R}_{p,q}^- = \mathfrak{R}_q^- + \mathfrak{T}_q^+\mathfrak{R}_{p,q-1}^-\left(\mathfrak{I} - \mathfrak{R}_q^+\mathfrak{R}_{p,q-1}^-\right)^{-1}\mathfrak{T}_q^-$$

$$\text{and} \quad \mathfrak{T}_{p,q}^+ = \mathfrak{T}_q^+\left(\mathfrak{I} + \mathfrak{R}_{p,q-1}^-\left(\mathfrak{I} - \mathfrak{R}_q^+\mathfrak{R}_{p,q-1}^-\right)^{-1}\mathfrak{R}_q^+\right)\mathfrak{T}_{p,q-1}^+,$$

where the matrix $\mathfrak{I}$ denotes the identity matrix of order $2N_s+1$. Numerical inspection of the behavior of the matrix $\mathfrak{I} - \mathfrak{R}_q^+\mathfrak{R}_{p,q-1}^-$ shows that it has a condition number of $\mathrm{O}(10)$ in most cases, so its inverse is always well-behaved. The recursive procedure

requires the initialisation $\mathfrak{R}^{\pm}_{1,1} = \mathfrak{R}^{\pm}_1$ and $\mathfrak{T}^{\pm}_{1,1} = \mathfrak{T}^{\pm}_1$ and runs until $\mathfrak{R}^{+}_{1,M}$ and $\mathfrak{T}^{\pm}_{1,M}$ are calculated.

We can also calculate the vectors of scattered amplitudes at each slab boundary $x = \xi_q$ in terms of the forcing vectors using the identities

$$\mathbf{A}^{+}_q = \left(\mathfrak{I} - \mathfrak{R}^{-}_{1,q}\mathfrak{R}^{+}_{q+1,M}\right)^{-1}\left(\mathfrak{T}^{+}_{1,q}\mathbf{A}^{+}_0 + \mathfrak{R}^{-}_{1,q}\mathfrak{T}^{-}_{q+1,M}\mathbf{A}^{-}_M\right), \quad \text{and} \tag{6.5a}$$

$$\mathbf{A}^{-}_q = \left(\mathfrak{I} - \mathfrak{R}^{+}_{q+1,M}\mathfrak{R}^{-}_{1,q}\right)^{-1}\left(\mathfrak{R}^{+}_{q+1,M}\mathfrak{T}^{+}_{1,q}\mathbf{A}^{+}_0 + \mathfrak{T}^{-}_{q+1,M}\mathbf{A}^{-}_M\right). \tag{6.5b}$$

7. Numerical results. In this section, we will show results that demonstrate how our model can be used to analyze regular and randomly perturbed scattering systems. The response of a system mostly depends on the relative size between wavelength, scatterer radii and relative distance between scatterers (spacing). We limit the number of parameters by non-dimensionalizing with respect to the wavenumber $k = \pi$ and setting the non-dimensional radius of all scatterers j to $a_j = 0.5$.

We establish the convergence of the numerical procedure with respect to the angular discretizations devised in §5, by ensuring the energy conservation relation

$$\int_{-\pi/2}^{\pi/2} \left|A^{+}_0(\chi)\right|^2 \mathrm{d}\chi = \int_{-\pi/2}^{\pi/2} \left|A^{-}_0(\chi)\right|^2 \mathrm{d}\chi + \int_{-\pi/2}^{\pi/2} \left|A^{+}_M(\chi)\right|^2 \mathrm{d}\chi \tag{7.1}$$

holds with an accuracy of 4 decimal places to limit the computational cost. Note that the two integrals on the right-hand side converge as $\mathrm{O}\left(N_s^{-3}\right)$, so the numerical scheme presented in the previous sections can provide higher accuracy if needed.

Consider an arrangement of 5 slabs of non-dimensional width $L = 2$, each containing 11 scatterers centered in the slab and with regular non-dimensional centre-to-centre spacing $s = 2$. We force the system with the incident spectrum $A^{\mathrm{In}}(\tau) = \cos\tau$, $-\pi/2 \leq \tau \leq \pi/2$, which is commonly used in the study of ocean wave spectra, for instance. Figure 2 shows the real part of the potential $\mathrm{Re}\,\phi$ through the rectangular lattice. In the left panel, the solution was computed using the WSA, while in the right panel we accounted for a portion of the evanescent plane wave components up to $\gamma = 2$. We observe significant discrepancies for the WSA particularly at the boundaries between slabs, where the wave field appears discontinuous. The discontinuity is removed in the second surface plot, suggesting that few evanescent components are required to characterize the wave field properly throughout the domain. Farther away from the scattering region, the discrepancies seem to persist, suggesting the WSA is not accurate when looking at far-field properties for this problem.

To confirm these qualitative observations we conduct a convergence analysis of the transmission coefficient with respect to the truncation parameter γ, with the transmission coefficient defined as

$$T = \sqrt{\left(\int_{-\pi/2}^{\pi/2} \left|A^{+}_M(\chi)\right|^2 \mathrm{d}\chi\right) \Big/ \left(\int_{-\pi/2}^{\pi/2} \left|A^{+}_0(\chi)\right|^2 \mathrm{d}\chi\right)}.$$

Figure 3 shows the transmission coefficient for $\gamma = 0$ to 3. It is clear that convergence is reached for $\gamma \approx 1$. A similar level of convergence was found throughout the simulations

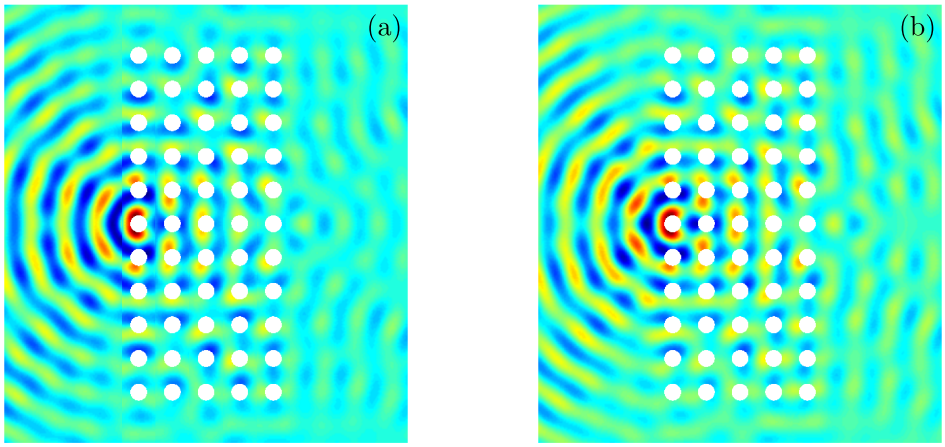

FIG. 2. *Real part of the potential ϕ for the scattering of an incident field with angular spectrum $A^{\mathrm{In}}(\tau) = \cos\tau$, $-\pi/2 \leq \tau \leq \pi/2$, by a 5 by 11 rectangular regular lattice of scatterers. The surface plots were obtained using (a) the WSA, i.e. $\gamma = 0$, and (b) a truncation parameter of evanescent components $\gamma = 2$.*

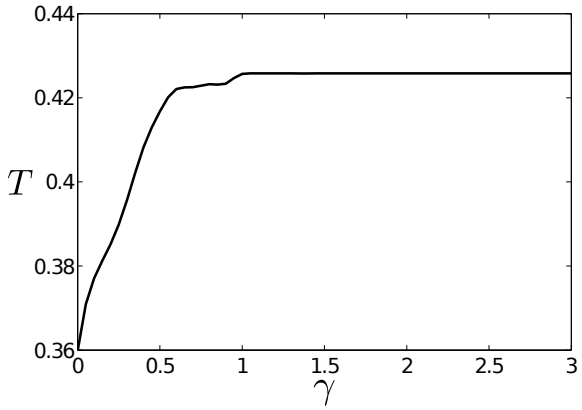

FIG. 3. *Convergence of the transmission coefficient with respect to the extent of evanescent wave components included in the simulations*

conducted as part of this investigation, so we set $\gamma = 2$ for the remainder of this study, unless otherwise specified. In particular, for a single slab, the far-field properties computed with the WSA would match those which include evanescent components, as the evanescent/traveling interactions only occur in multiple slab problems. Therefore, we take $\gamma = 0$ for the single slab problem.

We now investigate the relationship between a finite row of regularly spaced scatterers, and the corresponding infinite periodic row, using the method of Bennetts [2], which accommodates directional incident spectra. We consider a row of J scatterers with constant centre-to-centre spacing s, aligned vertically along the y-axis and arranged symmetrically with respect to the x-axis. The incident spectrum is the same as that in the previous example, which we note was also used in Bennetts [2] to analyze the response by infinite arrays.

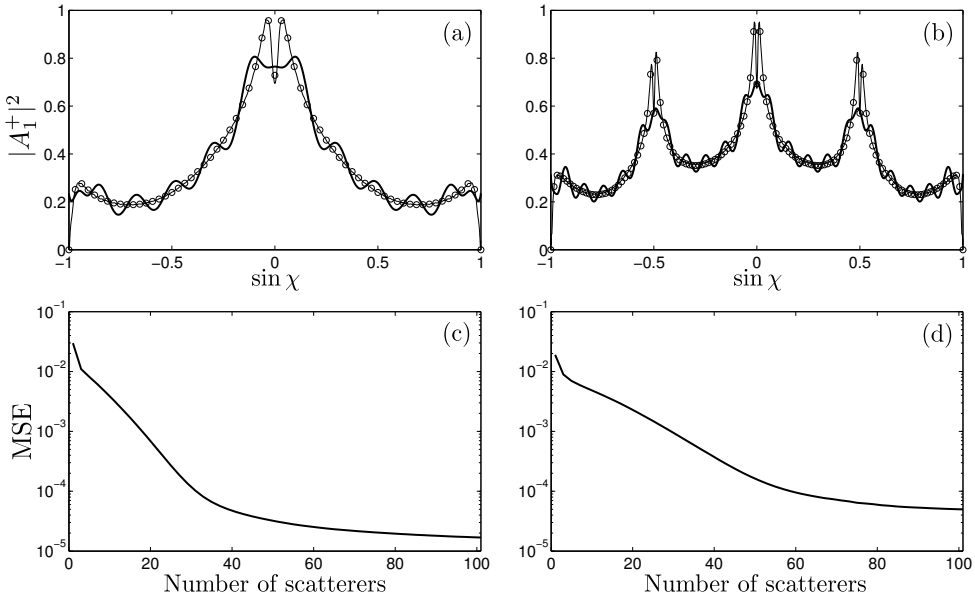

FIG. 4. *Angular spectrum of transmitted energy for a regular array of scatterers with spacing (a) $s = 2$ and (b) $s = 4$. In each panel, responses are given for $J = 11$ and 101 scatterers (thick and thin line, respectively), and compared to the infinite regular array response provided by Bennetts [2] (circles). The mean square error between finite and infinite array responses is plotted in the lower panels against the number of scatterers in the finite array for the two spacings considered.*

Figure 4(a,b) shows the angular spectrum of transmitted energy for spacings $s = 2$ and $s = 4$, respectively. In each panel, we compare the spectra computed from the finite array model with $J = 11$ and $J = 101$ (thick and thin lines, respectively), and the spectrum of the corresponding infinite array (circles). We find that for both spacings the finite array model with 101 scatterers gives a very good approximation of the infinite array response. This is all the more remarkable, observing that the methods used in our model and that of Bennetts [2] are substantially different. This comparison therefore helps validate the method devised in the current paper.

We can also examine the rate of convergence of the finite array model towards the infinite array with respect to the number of scatterers M. Figure 4(c,d) shows the mean square error (MSE) between the finite and infinite array transmitted energy spectra for increasing M. We find a quasi-exponential decay of the MSE between $J = 3$ and 31 for $s = 2$, and $J = 3$ and 51 for $s = 4$. This suggests that convergence towards the infinite array response is fast, so a good approximation of the behavior of an infinite array can be simulated reasonably easily with our model. We note that the MSE levels off below 10^{-4} in both cases, which is attributed to the finite array case converging to a solution slightly different from the infinite array solution, likely due to scattering near the edges of the finite array. Consequently, the approximation of the infinite array is only valid when the phase origin of the incident field is chosen in the middle of the finite array, so the edge effects are sufficiently small to have little influence on the reflected and transmitted spectra, also measured in the middle of the array.

The transmitted energy spectra plotted in Figure 4(a,b) display features that are worthy of comment. In particular, the resonances observed in these spectra are

characterized by double spikes at certain angles. For an infinite regular array, it is well established that scattered waves propagate at a finite number of well-defined angles, the so-called scattering angles, determined by the direction of the incident plane wave and the spacing between scatterers. The double spikes occur around the scattering angles excited for an incident plane wave in the normal direction. The normal direction carries the most energy in the incident spectrum considered here. It is interesting to observe that the transmitted field does not carry most its energy at these angles, but at angles nearby. When forced by an incident angular spectrum, all angular components superpose coherently, so interference mechanisms lead to cancellations at certain angles, which is the most reasonable explanation for the energy minimum at these scattering angles. Inspection of the reflected spectrum shows that sharp peaks occur at the scattering angles. These look similar to enhanced backscattering cones that form the basis of the coherent backscattering effect (weak localization) in weakly disordered media (Sheng [25]). This may indicate the physical nature of these resonances, although no references were found to confirm this hypothesis. A link to coherent backscattering is supported by the observation (not shown here) that the peaks and troughs (for reflected and transmitted spectra, respectively) occur consistently at these scattering angles regardless of the shape of the incident spectrum, e.g. for an asymmetric spectrum.

Our next goal is to investigate how random perturbation of a regular finite array of scatterers affects the angular spectrum of transmitted energy. For this purpose, we consider an array of 101 scatterers perturbed from their mean position on the y-axis, with regular spacing $s = 5$ and centered about the x-axis. The position of each scatterer j is then defined by $(x_j, y_j) = (0, (j - 51)s) + (\varepsilon d_x, \varepsilon d_y)$, for $1 \leq j \leq J$. The quantity ε is a random variable with uniform distribution in the interval $[-1, 1]$, and d_x and d_y define the non-dimensional maximum deviation from the mean position in the x and y directions, respectively.

We test the impulse response of the system for different degrees of disorder, for an impulse in the normal direction, i.e. $A^{\mathrm{In}}(\tau) = \delta(\tau)$. Discretizing the problem by taking $2N_s + 1$ samples of the angular domain (see §5), the response of the system is provided by the $(N_s + 1)^{\mathrm{th}}$ column of the reflection and transmission matrices defined by (5.1). We denote the transmitted impulse response by T^0 and compute the average $\langle |T^0| \rangle$ of 50 random realizations of the array, which is a sufficient number for this particular simulation. The results are displayed in figure 5 for different values of d_x and d_y, which control the amount of disorder imposed on the system.

Panel (a) shows the impulse response of the unperturbed array and, as expected, we can see spikes at the scattering angles (real solutions of $\sin\chi = 2l\pi/(ks)$, $l \in \mathbb{Z}$). Panels (b) and (c) show the response of the system for $d_x = 1$ and 2, respectively, and no perturbation in the y direction ($d_y = 0$). As d_x increases, the scattering angles $\sin\chi = \pm 4/5$ are gradually filtered out of the response, while the other spikes appear to be unaffected. Numerical results not shown here indicate that, for larger d_x, the scattering angles $\sin\chi = \pm 2/5$ eventually disappear from the response, too. Similar conclusions are found when the array is perturbed in the y direction only (see panels (d) and (f) obtained for $d_y = 1$ and 2, respectively), and of course in both directions.

With equal disorder in the x and y directions, scattering angles are filtered significantly more rapidly with a disturbance in the y direction. This is a sensible result due to the fact that scattering angles are determined by the spacing between scatterers, and the effect of a small perturbation on the spacing in the y and x direction is first and second order, respectively.

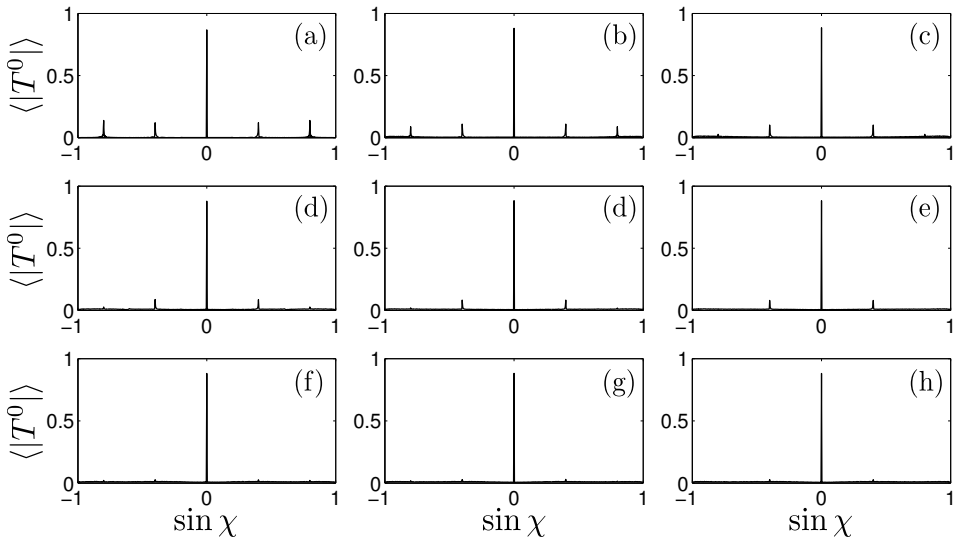

FIG. 5. *Effect of a random perturbation on the transmitted spectrum due to an impulse in the normal direction incident on an array composed of 101 scatterers. Ensemble averages of transmitted angular spectra are plotted in all panels with perturbation parameters $d_x = 0$, 1 and 2 in the panels of the first, second and third column, respectively, and $d_y = 0$, 1 and 2 in the panels of the three rows.*

With sufficient disorder in the system, we have shown that the array acts as a filter of the non-normal scattering angles, so that the perturbed row only transmits a wave in the same direction as the incident wave. This suggests that a directional spectrum of arbitrary shape traveling through the disordered row will transmit a spectrum of the same shape, but with reduced amplitude. To test this conjecture, we compute the transmitted and reflected spectra through the same array with perturbation parameters $d_x = 4$ and $d_y = 2$. We consider the three incident spectra:

$$A_1^{\mathrm{In}}(\tau) = \cos\tau,$$
$$A_2^{\mathrm{In}}(\tau) = \mathrm{H}(\tau + 3\pi/10) - \mathrm{H}(\tau + \pi/10),$$
$$A_3^{\mathrm{In}}(\tau) = \left(0.5\cos^{10}(\tau + \pi/4) + \cos^{10}(\tau - \pi/6)\right)\cos\tau,$$

for $-\pi/2 \leq \tau \leq \pi/2$. In the second incident spectrum, $\mathrm{H}(\tau) = 0$ if $\tau < 0$ and 1 if $\tau \geq 0$ is the Heaviside step function, which allows us to simulate the response to a discontinuous step. We estimate the ensemble average of the reflected and transmitted directional spectra from 5000 random realizations of the array.

Figure 6 shows the incident, reflected and transmitted spectra for the three forcings considered. We observe that in all cases the transmitted directional response preserves the shape of the incident spectrum, as conjectured from the analysis of impulse responses. In particular, the response to the step function $A_2^{\mathrm{In}}(\tau)$ (see (b)) is characterized by discontinuities in the transmitted spectrum at the same angles $\chi = -3\pi/10$ and $-\pi/10$. We observe further that the reflected spectra are all quasi-constant over the angular range, suggesting that randomizing the array produces a diffuse reflected field that is fully isotropic.

Inspection of the reflected field impulse response (not displayed here), shows that this diffuse state is predicted as the limiting behavior of the system under increas-

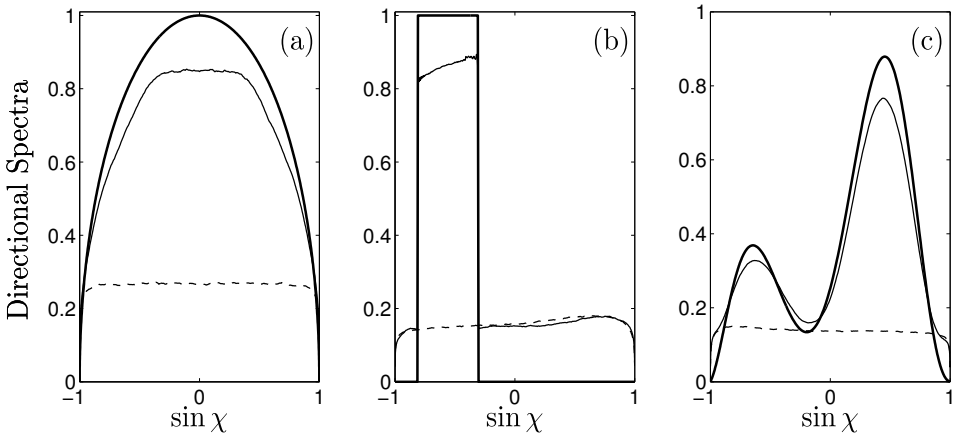

FIG. 6. *Incident (thick solid), transmitted (thin solid) and reflected (thin dashed) directional spectra due to an array composed of 101 scatterers perturbed randomly from the regular arrangement with spacing $s = 5$. Ensemble averages of each spectra are obtained from 5000 random realizations with perturbation parameters $d_x = 4$ and $d_y = 2$.*

ing degrees of random perturbation. Similarly to the transmitted response, spikes at the scattering angles are gradually filtered out by introducing more and more perturbations, although in this case the contribution of the normally-incident mode also disappears.

We now consider the response of a multiple row array composed of 10 slabs, computed using the WSA ($\gamma = 0$). We seek to validate the multiple row technique described in §6 for a regular arrangement of scatterers by comparing the transmitted energy directional spectrum with that provided by the infinite array model of Bennetts [2], restricted to the WSA. We fix the spacing between scatterers of each row to $s = 2$ and the spacing between rows to 2, and consider the incident field shown in figure 1b.

Figure 7 shows the transmitted energy spectra for 101 and 201 scatterers in each row (thick and thin lines respectively), compared to the infinite row arrays response of Bennetts [2] (circles). We see that 101-scatterer rows give a reasonably good approximation of the infinite row spectrum, although we can observe discrepancies at the peaks occurring at $\sin\chi \approx \pm 0.4$, ± 0.6 and ± 0.95. The two latter pairs of peaks are recovered by taking 201 scatterers in each row, but not the former one. Sensitivity tests (not shown) demonstrate that, as the number of scatterers in each row increases, more angular samples are needed to satisfy the energy conservation relation (7.1). As for the single row problem, the finite array solution does not seem to converge exactly to the infinite array solution, likely due to edge effects in the finite array case. A good approximation can be obtained with a few tens of scatterers, however, which captures the main features of the transmitted spectrum.

We observe, as for the single row problem, a significant drop of transmitted energy in the normal direction, which resembles the coherent backscattering effect that characterizes wave scattering in weakly disordered media.

We now seek to validate our method when disorder is introduced in the system. Foldy [11] proposed a simple approximation for the mean field in three-dimensional random media composed of sparsely concentrated identical isotropic scatterers. Two-dimensional versions of Foldy's effective media theory were subsequently given by Twersky [28], Aristégui and Angel [1] and Linton and Martin [17], for instance. Fol-

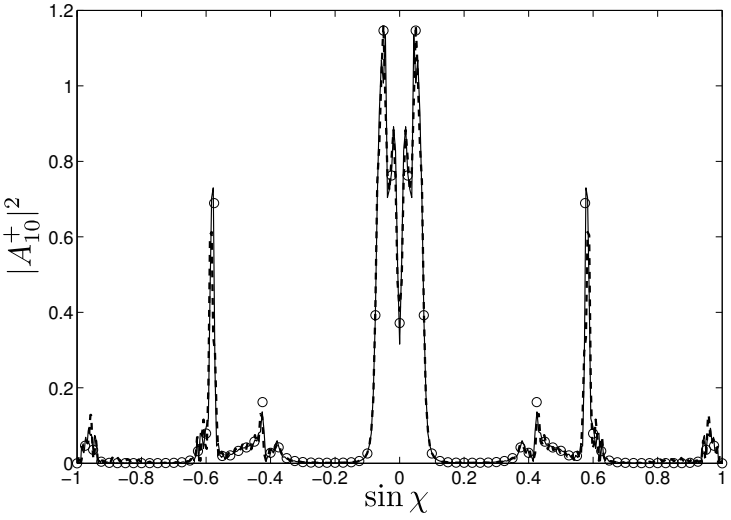

FIG. 7. *Directional spectrum of transmitted energy for a regular lattice composed of 10 rows of 101 (thick dashed line) and 201 (thin solid line) scatterers. The spacing between scatterers in a row is $s = 2$ and the spacing between rows is $L = 2$. The responses are compared to the infinite array transmitted energy spectrum provided by Bennetts [2] (circles).*

lowing the latter paper [17], the mean field through a semi-infinite random medium due to an incident plane wave with wavenumber k, angle τ with respect to the x-axis and amplitude $A^{\mathrm{In}}(\tau)$ (see integrand of (2.3)) is given by

$$\phi^{\mathrm{eff}}(x,y) = A^{\mathrm{In}}(\tau)U_0\,\mathrm{e}^{\,\mathrm{i}K(x\cos\varphi + y\sin\varphi)}, \quad \text{where} \tag{7.2}$$

$$K^2 = k^2 - 4\,\mathrm{i}n_0 g, \quad K\sin\varphi = k\sin\tau \quad \text{and} \quad U_0 = 2k\cos\tau/(k\cos\tau + K\cos\varphi).$$

The parameter n_0 defines the number of scatterer per unit area and should be small, while g describes the scattering strength of each isotropic scatterer. For finite size scatterers, it is given by $g = f(0)$, where

$$f(\theta) \approx \sum_{n=-N}^{N} \left(-\mathrm{J}_n^{'}(ka)/\mathrm{H}_n^{'}(ka)\right)\,\mathrm{e}^{\,in\theta}$$

is the far field pattern of each individual scatterer. The mean field due to a continuous incident directional spectrum as given by (2.3) is then obtained by integrating (7.2) with respect to τ with the understanding that U_0, K and φ are functions of τ.

We simulate a random medium with our model by considering an array of 50 slabs containing 101 scatterers of radius $a = 0.2$ each. As for the single slab problem, we define a finite regular array of scatterers in each slab and then perturb randomly the position of the scatterers. We fix the spacing in each row to $s = 2$ and the width of all slabs to $L_q = 5$, $1 \le q \le 50$, so that $n_0 = 0.1$. We consider a forcing with directional spectrum $A^{\mathrm{In}}(\tau) = \cos\tau$, as defined in figure 1b. In each slab q, scatterers have their position defined by $(x_j, y_j) = (2(q-1), 2(j-51)) + (\varepsilon d_x, \varepsilon d_y)$, $1 \le j \le J_q$, with $d_x = L_q/2 - a$ and $d_y = s/2 - a$ to avoid overlap.

We perform Monte Carlo simulations to estimate the modulus of the mean field through the array along the x-axis $|\langle\phi(x,0)\rangle|$. For each random realisation of the array,

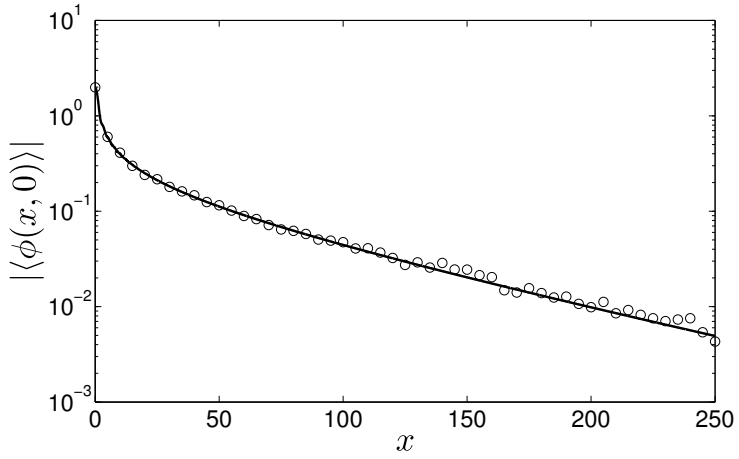

FIG. 8. *Modulus of the mean wave field along the x-axis in a random medium composed of small identical scatterers. The mean field is estimated using Foldy's approximation as described in Linton and Martin [17] (solid line) and as the ensemble average of 1000 random realisations of a finite array of 5050 scatterers using the slab-clustering method described in this paper (circles).*

we calculate the field at each slab boundary using (7.1) with $y = 0$, and we average over 1000 realisations of the array. Figure 8 shows the modulus of the mean field through the medium using Foldy's approximation and the slab-clustering technique. We observe good agreement between the two approaches, providing another validation of the method devised in this paper.

The effective medium theory of Foldy can only estimate the mean field in a random medium $|\langle\phi(x,y)\rangle|$, which is in general different compared to the mean of the individual (physical) fields $\langle|\phi(x,y)|\rangle$ (see, e.g., Wu [32]). Only the latter can be used to estimate the evolution of the wave properties, e.g. attenuation of energy and changes in directional spreads, as experienced by individual fields and which concern most physical applications. Consequently, we do not discuss mean fields further.

We now consider the response of an array composed of 50 slabs containing 101 scatterers of radius $a = 0.5$ each, and introduce a random perturbation on the position of the scatterers for different values of $0 \leq d_x, d_y \leq 0.5$. The reflected and transmitted directional spectra $A_0^-(\chi)$ and $A_{50}^+(\chi)$ are displayed in figures 9a and 9b, respectively, for the regular array case ($d_x = d_y = 0$). The spectra contain many spikes and irregularities as a result of complicated coherent interactions within this large array (5050 scatterers). Of particular interest is the spike in the reflected spectrum in the normal direction and the corresponding minimum at the same angle in the transmitted spectrum. This behavior is analogous to that observed in the response of a single slab, where minima in the transmitted spectrum at the scattering angle were observed in the periodic row case. For the present multiple slab array, the only scattering angle is the normal direction, indicating that the minimum there may also be linked to the coherent backscattering effect.

We introduce random perturbations in the array in figures 9c and 9d, where we show the average reflected and transmitted spectra, respectively, for an ensemble of 1000 realizations of the array. The response of the system is given for 3 different types of perturbation: (i) in the x direction only ($d_x = 0.5$ and $d_y = 0$), (ii) in the y direction only ($d_x = 0$ and $d_y = 0.5$), and (iii) in both directions ($d_x = d_y = 0.5$).

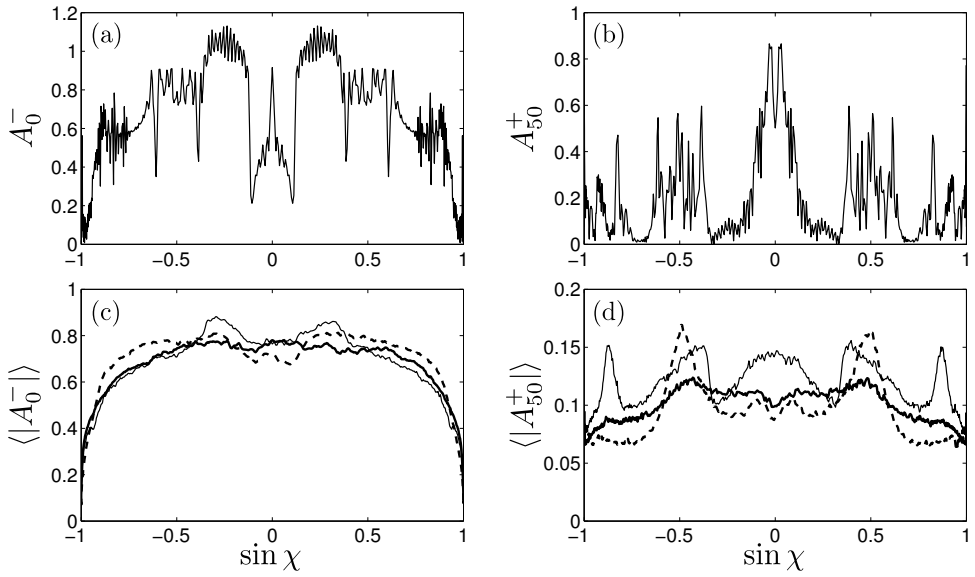

FIG. 9. *(a,c) Reflected and (b,d) transmitted spectra for an array composed of 50 slabs of 101 scatterers, under an incident spectrum as defined in figure 1b. Responses are displayed for (a,b) the regular array with constant spacing $s = 2$ and (c,d) an ensemble of 1000 random realizations with perturbation parameters (i) $d_x = 0.5$ and $d_y = 0$ (thick dashed); (ii) $d_x = 0$ and $d_y = 0.5$ (thin solid); and (iii) $d_x = d_y = 0.5$ (thick solid).*

The reflected spectra are similar for all three cases. They are almost constant over a large portion of the angular range. They characterize a quasi-isotropic diffuse state for which wave energy can be reflected in all directions with equal probability.

The transmitted spectra, however, preserve some of the structure of the regular case. In cases (i) and (ii), we observe several peaks indicating preferred directions of propagation of the transmitted energy. The peaks occur in sub-intervals of the angular range where the regular array transmits more energy (see figure 9a), suggesting that the shape of the spectra is mainly governed by similar coherent interactions as those observed for the regular array. In particular, the spacing between the rows is constant in case (ii), which provides a regularity in the array that allows the wave field to resonate in certain directions. More evidence towards this conjecture will be given shortly. In case (iii), more perturbation is introduced in the system and the transmitted spectrum is more uniform and smooth across the angular range. The degree of disorder is now sufficient to filter most resonating features associated with the regular array, although maxima can still be observed for $\sin\chi \approx \pm 0.45$.

To understand how the reflected and transmitted spectra form, we plot the left- and right-traveling spectra at the interfaces between rows 10 and 11, $\langle |A_{10}^{\pm}(\chi)| \rangle$, and between rows 30 and 31, $\langle |A_{30}^{\pm}(\chi)| \rangle$, in figure 10. The spectra for cases (i) and (iii) look remarkably similar and travel quasi-isotropically through the array. This behavior indicates that the shape of the transmitted spectra observed in figure 9d form closer to the end of the array. Inspection of the directional spectra deeper in the multiple row array (not displayed here) shows that the peaks seen in the transmitted spectrum form after the 40th row. This observation suggests that the transmitted spectrum is strongly influenced by the boundary rows of the array.

In case (ii), perturbations are introduced in the y direction only, so the spacing

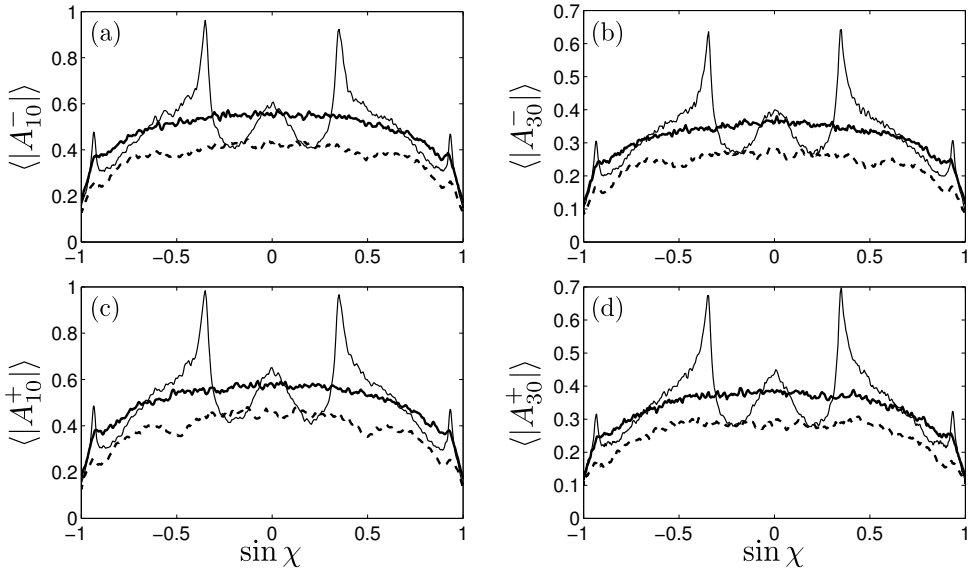

FIG. 10. *Ensemble average of directional spectra after (a,c) 10 slabs and (b,d) 30 slabs, for the situation considered in figure 9. The left- and right-traveling spectra are shown in panels (a,b) and (c,d), respectively. Results are given for different degrees of disorder with thick dashed, thin solid and thick solid lines corresponding to the perturbation parameters of cases (i), (ii) and (iii), respectively, considered in figure 9.*

between rows is the same. This allows resonant peaks to persist through the array as observed in figure 10, unaffected by the disorder introduced within each row. This behavior contrasts with the outcome of the single row analysis, where perturbations in the y direction eliminated resonant behaviors more strongly than perturbations in the x direction. The constant row spacing of this array suggests a relation to Bragg scattering, which occurs in regular lattices. Interestingly, the peaks observed in this case are not present in the reflected spectrum, although we can observe them from the second row onwards (not shown here).

As a final observation, we note that, apart from the boundary rows within the array, the shape of the directional spectrum is quasi-constant in disordered multiple-row arrays, while localization causes wave energy to decay exponentially. The regular array case shows a similar behavior (not displayed here), although wave energy does not decay in the same way.

8. Concluding remarks. A new method has been proposed to describe the multiple scattering of waves by a large finite array of circular obstructions in two dimensions and the concomitant evolution of directional wave properties through the array. The method was presented for a canonical planar acoustic problem with sound-hard scatterers. The wave forcing consists of a directional spectrum of plane waves, i.e. a superposition of plane waves with amplitudes that vary continuously with their direction of propagation. The method allowed us to simulate the response of regular and randomly perturbed arrays, and to investigate the effect of the disorder on the directionality of the scattered field.

Given an arbitrary array, we define a slab that contains it. We are able to find semi-analytical expressions for the reflected and transmitted fields, also defined as

directional spectra of plane waves, by combining the multipole method for multiple scattering by finite arrays and the integral transform of cylindrical harmonics into directional spectra of plane waves. Discretizing the angular domain, we obtain a scattering matrix for the slab. The extension to multiple slabs follows from the S-matrix method, and provides a directional spectrum representation of the wave field at each slab boundary, allowing us to track its evolution through the array. Numerical limitations related to the number of scatterers within each slab exist, although the FMM could be used as a remedy. Instead, increasing the number of slabs with our method allows us to solve multiple scattering problems for very large arrays, e.g. $\mathrm{O}\left(10^3\text{–}10^4\right)$ scatterers.

Numerical simulations were conducted to investigate (a) the validity of the wide-spacing approximation (WSA) for multiple slabs, (b) the approximation of the infinite single- or multiple-row response by finite rows/slabs of regularly spaced scatterers, (c) the attenuation of the mean field through a random array using Monte Carlo simulations and the analytical Foldy's approximation, and (d) the effect of randomly perturbing the position of each scatterer from its regular arrangement on the directional properties of the wave field traveling through the array. The main findings are summarized below.

1. The WSA does not capture accurately the reflected and transmitted properties for multiple slabs, due to the traveling/evanescent wave interactions that occur between slabs. Few evanescent wave components are needed to compute the solution with high accuracy.

2. The transmitted energy spectrum due to an infinite row (provided by Bennetts [2]) is approximated accurately by the corresponding finite regular row, therefore validating our solution method. For multiple rows, we found reasonably good agreement as most features of the transmitted spectrum are captured, although numerical limitations for an increasing number of scatterers in each row impede the convergence towards the infinite multiple-row array response.

3. Further validation of our method was obtained for random arrays, where a comparison of the mean field through a large random array between Monte Carlo simulations with our method and Foldy's approximation for the effective properties of semi-infinite random media showed very good agreement.

4. Under random perturbations in the position of regularly spaced scatterers in a finite row, we analyzed the ensemble average of the transmitted spectrum due to impulse forcing in the normal direction. We found that energy in the direction of the scattering angles is gradually filtered out, except that in the direction of the forcing, for increasing levels of disorder, while the reflected spectrum becomes isotropic. This observation suggests that for sufficient disorder in a single row, the transmitted spectrum has the same shape as the incident spectrum. This conjecture was validated for 3 different incident spectra.

5. The directional spectra through a 50-slab array, each containing 101 randomly perturbed scatterers, were computed from an average of random realizations of the array. We found that the reflected spectrum is quasi-isotropic, while the transmitted spectrum exhibits resonances at certain angles that depend on the type of perturbation introduced. In contrast, the directional spectrum through the array and sufficiently far from the boundary rows evolves without such resonances, except when the row spacing is fixed. We also found that the shape of the spectra remains quasi-constant except close to the boundary rows, a feature that was also observed for a regular multiple-row array.

Appendix A. The forcing experienced by obstruction j is the superposition of the incident wave ϕ_j^{In} and the scattered waves due to all obstructions, except j. The total wave field is then given by

$$\phi(r_j,\theta_j) = \phi^{\mathrm{In}}(r_j,\theta_j) + \phi_j^{\mathrm{S}}(r_j,\theta_j) + \sum_{p=1,\,p\neq j}^{J} \phi_p^{\mathrm{S}}(r_p(r_j,\theta_j),\theta_p(r_j,\theta_j)). \tag{A.1}$$

We invoke Graf's addition theorem (see Martin [18], Theorem 2.12) to express the multipole expansion of ϕ_p^{S} in the local coordinates of obstruction j, i.e.

$$\phi_p^{\mathrm{S}}(r_j,\theta_j) = \sum_{n=-\infty}^{\infty} \left(\sum_{s=-\infty}^{\infty} c_s^{(p)} \mathrm{H}_{s-n}(kR_{pj})\, \mathrm{e}^{\,\mathrm{i}(s-n)\vartheta_{pj}} \right) \mathrm{J}_n(kr_j)\, \mathrm{e}^{\,\mathrm{i}n\theta_j}, \tag{A.2}$$

with (R_{pj},ϑ_{pj}) the polar coordinates of the centre of obstruction j in the local system associated with obstruction p. Note that (A.2) is valid for $r_j \leq R_{pj}$, although this condition is automatically satisfied if the obstructions do not overlap. We can now apply the boundary condition (2.2) on Γ_j, using (2.5), (2.7), (A.1) and (A.2). Truncating infinite sums to include $2N+1$ modes only, we obtain

$$-c_n^{(j)} \frac{\mathrm{H}_n'(ka_j)}{\mathrm{J}_n'(ka_j)} - \sum_{p=1,\,p\neq j}^{J} \sum_{s=-N}^{N} c_s^{(p)} \mathrm{H}_{s-n}(kR_{pj})\, \mathrm{e}^{\,\mathrm{i}(s-n)\vartheta_{pj}} = f_n^{(j)}, \tag{A.3}$$

for all n, $-N \leq n \leq N$, and j, $1 \leq j \leq J$. This is a system of $M(2N+1)$ algebraic equations, which can be solved numerically for the $c_n^{(j)}$. Symmetries in the system can be used to reduce the number of Hankel function evaluations, which are computationally expensive. The second term of the left-hand side in (A.3), related to multiple scattering effects, is generally expensive to compute. It could be accelerated using the FMM, based on the far-field expansions of cylindrical harmonics (see, e.g., Lai et al. [15]). Achieving maximal efficiency is not the focus of this paper, however, so we do not consider FMM acceleration here.

REFERENCES

[1] C. Aristégui and Y. C. Angel, *New results for isotropic point scatterers: Foldy revisited*, Wave Motion, 36 (2002), pp. 383–399.

[2] L. G. Bennetts, *Wave attenuation through multiple rows of scatterers with differing periodicities*, SIAM J. Appl. Math., 71 (2011), pp. 540–558.

[3] L. G. Bennetts, M. A. Peter, V. A. Squire, and M. H. Meylan, *A three dimensional model of wave attenuation in the marginal ice zone*, J. Geophys. Res., 115 (2010), p. C12043.

[4] L. G. Bennetts and V. A. Squire, *Wave scattering by multiple rows of circular ice floes*, J. Fluid Mech., 639 (2009), pp. 213–238.

[5] R. Borghi, F. Frezza, M. Santarsiero, C. Santini, and G. Schettini, *A quadrature algorithm for the evaluation of a 2D radiation integral with a highly oscillating kernel*, J. Electromagnet. Wave., 14 (2000), pp. 1353–1370.

[6] L. Brillouin, *Wave propagation in periodic structures: electric filters and crystal lattices*, McGraw-Hill Book company, Inc., 1946.

[7] L.-W. Cai and J. H. Williams Jr, *Large-scale multiple scattering problems*, Ultrasonics, 37 (1999), pp. 453–462.

[8] H. Cheng, W. Crutchfield, Z. Gimbutas, L. Greengard, J. Huang, V. Rokhlin, N. Yarvin, and J. Zhao, *Remarks on the implementation of the wideband fmm for the helmholtz equation in two dimensions*, Contemp. Math., 408 (2006), pp. 99–110.

[9] G. Cincotti, F. Gori, M. Santarsiero, F. Frezza, F. Furno, and G. Schettini, *Plane wave expansion of cylindrical functions*, Opt. Commun., 95 (1993), pp. 192–198.

[10] N. P. K. Cotter, T. W. Preist, and J. R. Sambles, *Scattering-matrix approach to multilayer diffraction*, J. Opt. Soc. Am. A, 12 (1995), pp. 1097–1103.
[11] L. L. Foldy, *The multiple scattering of waves. i. general theory of isotropic scattering by randomly distributed scatterers*, Phys. Rev., 67 (1945), pp. 107–119.
[12] F. Frezza, L. Pajewski, C. Ponti, and G. Schettini, *Scattering by dielectric circular cylinders in a dielectric slab*, J. Opt. Soc. Am. A, 27 (2010), pp. 687–695.
[13] H. Kagemoto and D. K. P. Yue, *Interactions among multiple three-dimensional bodies in water waves: an exact algebraic method*, J. Fluid Mech., 166 (1986), pp. 189–209.
[14] D. Y. K. Ko and J. R. Sambles, *Scattering matrix method for propagation of radiation in stratified media: attenuated total reflection studies of liquid crystals*, J. Opt. Soc. Am. A, 5 (1988), pp. 1863–1866.
[15] J. Lai, M. Kobayashi, and L. Greengard, *A fast solver for multi-particle scattering in a layered medium*, Opt. Express, 22 (2014), pp. 20481–20499.
[16] L. Li, *Formulation and comparison of two recursive matrix algorithms for modeling layered diffraction gratings*, J. Opt. Soc. Am. A, 13 (1996), pp. 1024–1035.
[17] C. M. Linton and P. A. Martin, *Multiple scattering by random configurations of circular cylinders: Second-order corrections for the effective wavenumber*, J. Acoust. Soc. Am., 117 (2005), pp. 3413–3423.
[18] P. A. Martin, *Multiple scattering: interaction of time-harmonic waves with N obstacles*, no. 107, Cambridge University Press, 2006.
[19] R. C. McPhedran, L. C. Botten, A. A. Asatryan, N. A. Nicorovici, P. A. Robinson, and C. M. de Sterke, *Calculation of electromagnetic properties of regular and random arrays of metallic and dielectric cylinders*, Physical Review E, 60 (1999), p. 7614.
[20] R. F. Millar, *Plane wave spectra in grating theory Part IV: scattering by a finite grating of identical cylinders*, Can. J. Phys., 42 (1964), pp. 2395–2410.
[21] M. G. Moharam, D. A. Pommet, E. B. Grann, and T. K. Gaylord, *Stable implementation of the rigorous coupled-wave analysis for surface-relief gratings: enhanced transmittance matrix approach*, J. Opt. Soc. Am. A, 12 (1995), pp. 1077–1086.
[22] W. J. Parnell and P. A. Martin, *Multiple scattering of flexural waves by random configurations of inclusions in thin plates*, Wave Motion, 48 (2011), pp. 161–175.
[23] M. A. Peter and M. H. Meylan, *Water wave scattering by vast field of bodies*, SIAM J. Appl. Math., 70 (2009), pp. 1567–1586.
[24] C. Schwartz and L. F. DeSandre, *New calculational technique for multilayer stacks*, Appl. Opt., 26 (1987), pp. 3140–3144.
[25] P. Sheng, *Introduction to wave scattering, localization and mesoscopic phenomena*, vol. 88, Springer, 2006.
[26] A. Sommerfeld, *Partial differential equations in physics*, vol. 1, Academic press, 1949.
[27] V. Twersky, *Multiple scattering of radiation by an arbitrary configuration of parallel cylinders*, J. Acoust. Soc. Am., 24 (1952), pp. 42–46.
[28] ———, *On scattering of waves by random distributions. i. free-space scatterer formalism*, J. Math. Phys., 3 (1962), pp. 700–715.
[29] ———, *Scattering of waves by two objects*, in Electromagnetic Waves, R. E. Langer, ed., 1962.
[30] J. O. Vasseur, P. A. Deymier, B. Chenni, B. Djafari-Rouhani, L. Dobrzynski, and D. Prevost, *Experimental and theoretical evidence for the existence of absolute acoustic band gaps in two-dimensional solid phononic crystals*, Physical Review Letters, 86 (2001), p. 3012.
[31] P. Wadhams, V. A. Squire, J. A. Ewing, and R. W. Pascal, *The effect of the marginal ice zone on the directional wave spectrum of the ocean*, J. Phys. Oceanogr., 16 (1986), pp. 358–376.
[32] R.-S. Wu, *Mean field attenuation and amplitude attenuation due to wave scattering*, Wave Motion, 4 (1982), pp. 305–316.
[33] P. Yeh, *Electromagnetic propagation in birefringent layered media*, J. Opt. Soc. Am. A, 69 (1979), pp. 742–756.